

Continuum-discretized coupled-channel calculations for ${}^6\text{Li}$ fusion reactions with closed channels

Wendi Chen¹, D.Y. Pang¹, Hairui Guo², Ye Tao², Weili Sun² and Yangjun Ying²

¹*School of Physics, Beihang University, Beijing 100191, People's Republic of China*

²*Institute of Applied Physics and Computational Mathematics, Beijing 100094, People's Republic of China*

(Dated: June 13, 2023)

Fusion reactions induced by the weakly bound nucleus ${}^6\text{Li}$ with targets ${}^{28}\text{Si}$, ${}^{64}\text{Ni}$, ${}^{144}\text{Sm}$ and ${}^{209}\text{Bi}$ at energies around the Coulomb barrier are investigated within a three-body model where ${}^6\text{Li}$ is described with an $\alpha + d$ cluster model. The total fusion (TF) cross sections are calculated with the continuum-discretized coupled-channel (CDCC) method and the complete fusion (CF) cross sections are extracted through the sum-rule model. The calculations demonstrate that (i) for the TF cross section calculations, the continuum states up to 40 MeV are found to be necessary, which corresponds to the inclusion of closed channels for light and medium mass targets, such as ${}^{28}\text{Si}$, ${}^{59}\text{Co}$ and ${}^{144}\text{Sm}$, (ii) the converged CDCC results for TF cross section at energies above the Coulomb barrier are almost the same as single channel results in which the continuum coupling effect is neglected, and (iii) the continuum coupling strongly influences partial wave fusion cross sections and the closed channels play a significant role in the improvement of the description of the CF cross sections at energies below the Coulomb barrier for the ${}^6\text{Li}+{}^{28}\text{Si}$, ${}^{59}\text{Co}$ and ${}^{144}\text{Sm}$ systems.

I. INTRODUCTION

Reactions induced by weakly bound projectiles have been extensively investigated in the last few decades [1–5]. In these reactions, breakup is a very important reaction channel and has a strong coupling effect on elastic scattering, inelastic scattering, transfer and fusion channels. In particular, special attention has been given to the continuum coupling effects on fusion reactions both theoretically and experimentally [6–13]. Among the stable weakly bound nuclei, ${}^6\text{Li}$ has always been of interest, as it has only one bound state with a low separation energy of 1.47 MeV for breaking up into α and d fragments. So far, many experiments for ${}^6\text{Li}$ -induced fusion reactions have been reported, with targets varying from light nuclei, such as ${}^{27}\text{Al}$ [14] and ${}^{28}\text{Si}$ [15], to heavy nuclei, such as ${}^{197}\text{Au}$ [16] and ${}^{209}\text{Bi}$ [7, 17]. But the experimental data are still far from being fully understood.

Owing to the low binding energy of the projectile, there is a high probability that the projectile breaks into two or more fragments. In such cases, two kinds of fusion processes in the collisions of weakly bound nuclei have emerged from previous investigations, namely the complete fusion (CF) and the incomplete fusion (ICF). CF occurs when the whole weakly bound projectile is captured by the target. ICF occurs when some fragments of the projectile are captured and others escape. The sum of CF and ICF amounts to the total fusion (TF).

It is a great challenge to develop a realistic theory to describe the fusion process of weakly bound nuclei. Up to now, various theoretical approaches have been presented, among which the continuum discretized coupled-channel (CDCC) method has been the most popular one in making realistic predictions for the fusion reactions induced by weakly bound nuclei [5, 11–13, 18–23], as it can effectively take the continuum coupling effect into account. For ${}^6\text{Li}$, many researchers [11, 12, 22] have adopted the CDCC method to calculate its TF cross sections. How-

ever, it is hard to evaluate the contributions from CF and ICF processes to TF cross sections for ${}^6\text{Li}$ as its breakup fragments are both charged and their masses are comparable. Recently, a direct approach based on the CDCC method to evaluate the CF and ICF cross sections for ${}^{6,7}\text{Li}$ fusion reactions was developed by Lubian et al. [13, 23, 24], in which the probabilities of CF and ICF processes were obtained by integrating the scattering wave functions with different matrix elements of coupled-channel equations. They obtained a reasonable agreement between theory and experiment for ${}^{6,7}\text{Li}$ fusion with heavy nuclei. On the other hand, Lei and Moro [5] obtained the CF cross sections for ${}^{6,7}\text{Li}+{}^{209}\text{Bi}$ indirectly by subtracting the cross sections of elastic breakup, nonelastic breakup and inelastic scattering from the total reaction cross section. Their results were in satisfactory agreement with experimental CF data, too. In addition, a different approach was developed by Parkar et al. [21] in which the CF, ICF and TF cross sections are obtained by three CDCC calculations with different short-range imaginary potentials. Their calculated results for ${}^{6,7}\text{Li}+{}^{198}\text{Pt}$ and ${}^{209}\text{Bi}$ were also in reasonable agreement with experimental data. These studies are all about ${}^6\text{Li}$ fusion with heavy targets. Fusion reactions of ${}^6\text{Li}$ with light and medium mass nuclei are still rare.

In many cases, the convergence of CDCC calculations is not easy to be achieved when they are applied in evaluating the fusion reaction cross sections. To overcome this problem, Diaz-Torres et al. [11] neglected the imaginary parts of off-diagonal couplings and only kept the imaginary parts in diagonal couplings in their study of ${}^6\text{Li}$ fusion reactions. Similarly, Lubian et al. [13] neglected the imaginary parts of matrix elements between bound and breakup channels. In these works, the maximum energy of the continuum states, ε_{max} , for ${}^6\text{Li}$ was set to be 6.0–8.0 MeV. It is far lower than the threshold energy of the continuum states, $\varepsilon_{th}=E_{cm}-\varepsilon_b$, where E_{cm} is the incident energy in the centre of mass system and ε_b is the

separation energy of α and d in the ground state ${}^6\text{Li}$.

It is well known that closed channels, whose channel energies are negative, play an important role in the low-energy reaction induced by weakly bound nuclei. Yahiro et al [25] have discussed the coupling effect of closed channels on deuteron elastic scattering, which is visible for $d+{}^{58}\text{Ni}$ reaction at low incident energy. Ogata and Yoshida [26] have reexamined the calculations for deuteron elastic breakup cross sections on ${}^{12}\text{C}$ and ${}^{13}\text{Be}$ at low incident energies. They pointed out that closed channels are required for CDCC calculations to obtain good agreement with the result of Faddeev-Alt-Grassberger-Sandhas theory, in which the three-body problem is exactly solved. Very recently, we [27] presented a CDCC analysis for ${}^6\text{Li}+{}^{59}\text{Co}$ reactions at energies around the Coulomb barrier and found that the ε_{max} for ${}^6\text{Li}$ should be at least 50.0 MeV to obtain converged elastic breakup reaction cross section. Therefore, it is worthy of reexamining the fusion cross section calculations by increasing ε_{max} to check whether the continuum coupling effect is completely taken into account.

Furthermore, as a semi-classical approach, the sum-rule model [28–32] is adopted to distinguish the CF and ICF processes. According to this model, CF and ICF occur at lower and higher angular momenta respectively. It is of interest to study the continuum coupling effect on ${}^6\text{Li}$ complete fusion with this model, as it can give a clear and simple dependence of CF cross sections on angular momenta and incident energy. Meanwhile, it can be applied to the ${}^6\text{Li}$ fusion reactions with different targets, enabling us to investigate the influence of targets on CF.

In the present work, we study the coupling effect of continuum states on TF and CF cross sections for ${}^6\text{Li}$ fusion with ${}^{28}\text{Si}$, ${}^{64}\text{Ni}$, ${}^{144}\text{Sm}$ and ${}^{209}\text{Bi}$ targets at energies around the Coulomb barrier. Particular attention is given to the reexamination of CDCC calculations for ${}^6\text{Li}$ total fusion cross sections, where the numerical convergence problem should be solved by increasing ε_{max} . With the converged calculated results, the CF cross sections will be extracted by the sum-rule model to study the dependencies of CF process on breakup channels and targets. The coupling effects of open and closed channels will also be discussed.

The paper is organized as follows. The formalism is given in Sec. II. Reexamination of ${}^6\text{Li}$ CDCC calculations for total fusion is presented in Sec. III. Sec. IV discusses the coupling effect of continuum states on TF and CF cross sections in detail. Finally, the summary and conclusion are given in Sec. V.

TABLE I. Parameters of the effective $\alpha - d$ potential $V_{\alpha-d}$ [27] in Woods-Saxon form. This potential is l -dependent. Its nuclear radius R_N and Coulomb radius R_C are both 2.1 fm. The diffuseness parameter a is 0.65 fm. V_0 and V_{so} represent the depths of the central and spin-orbit potentials respectively and their units are MeV.

l	0	1	2
V_0	67.69	63.90	65.33
V_{so}	0.00	5.72	4.78

TABLE II. Calculated resonance energies ε_{res}^{cal} and widths Γ_{res}^{cal} compared with experimental value ε_{res}^{exp} and Γ_{res}^{exp} [33]. Their units are MeV.

State	ε_{res}^{cal}	Γ_{res}^{cal}	ε_{res}^{exp}	Γ_{res}^{exp}
3^+	0.710	0.084	0.716	0.024
2^+	3.00	1.12	2.84	1.30
1^+	4.24	2.93	4.18	1.50

II. THEORETICAL MODEL

A. $\alpha+d$ cluster model for ${}^6\text{Li}$

${}^6\text{Li}$ is described in $\alpha+d$ cluster model. Its internal wave function is written as

$$\psi = \mathcal{A} \left\{ \varphi(\alpha) [\varphi_s(d) \otimes \chi_l(\vec{r})]_I^M \right\}, \quad (1)$$

where \mathcal{A} means the antisymmetrization of the nucleons. $\varphi(\alpha)$ and $\varphi_s(d)$ are the intrinsic wave functions of α and d clusters respectively. \vec{r} is the relative coordinate between two clusters. χ_l represents the $\alpha - d$ relative motion with angular momentum l , which couples with the spin of deuteron cluster, s , to form the total spin I and its projection M .

In the present work, a simple version of the orthogonality condition model [37–40] is used to calculate the ${}^6\text{Li}$ internal wave function ψ . The effects of the antisymmetrization of nucleons are taken into account approximately by employing an effective $\alpha - d$ potential, $V_{\alpha-d}$, and excluding the deepest bound state as the forbidden state. Therefore, ψ is calculated by solving a Schrodinger equation with $V_{\alpha-d}$ [27], which is l -dependent. $V_{\alpha-d}$ are parameterized by the Woods-Saxon form [41], including the central and spin-orbit potentials. Its parameters for $l=0, 1$ and 2 are listed in Table I. $V_{\alpha-d}$ can well reproduce the binding energy of 1.47 MeV ($l=0, s=1$ and $I^\pi=1^+$) as well as the $3^+, 2^+$ and 1^+ resonance states in D -wave continuum. The calculated resonance energies and widths are shown in Table II, compared with the experimental data [33]. $V_{\alpha-d}$ also describes the low-energy $\alpha - d$ scattering phase shifts well, shown in Fig 1 as a function of the relative $\alpha - d$ energy in centre of mass system ε .

The spacial wave functions of the d and α clusters are

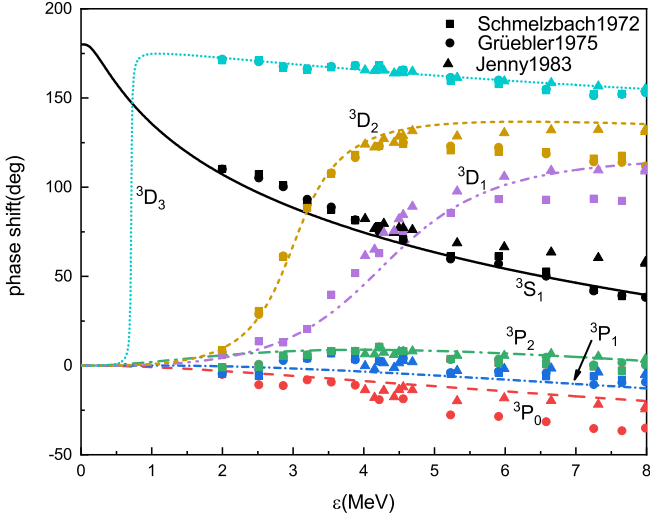


FIG. 1. (Color online) Calculated $\alpha-d$ scattering phase shift with $V_{\alpha-d}$ [27], shown as a function of the relative $\alpha-d$ energy in centre of mass system, ε . Experimental data are taken from Schmelzbach et al. [34] (squares), Gruebler et al. [35] (circles) and Jenny et al. [36] (triangles).

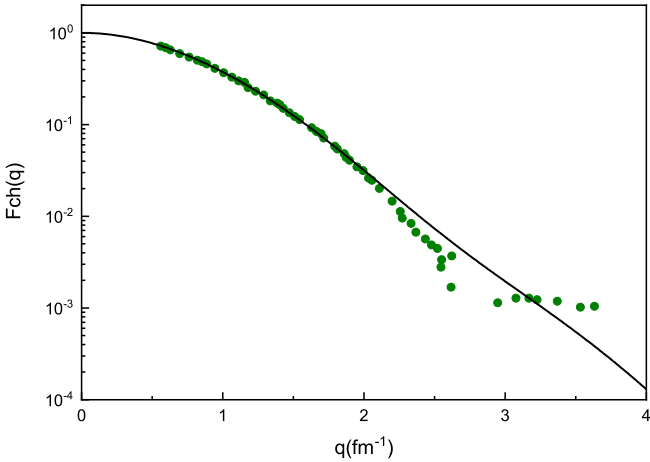


FIG. 2. (Color online) Calculated charge form factors of elastic electron scattering by ${}^6\text{Li}$, compared with the experimental data [42].

assumed to be $(1s)^2$ and $(1s)^4$ harmonic oscillator shell model wave functions with different oscillator constants β_d and β_α respectively ($\beta = m\omega/\hbar$), and expressed as

$$\begin{aligned} \varphi(d) &= N_d \exp \left[-\frac{\beta_d}{2} \sum_{i \in d} (\vec{r}_i - \vec{R}_d)^2 \right], \\ \varphi(\alpha) &= N_\alpha \exp \left[-\frac{\beta_\alpha}{2} \sum_{i \in \alpha} (\vec{r}_i - \vec{R}_\alpha)^2 \right] \end{aligned} \quad (2)$$

where $\beta_d=0.390 \text{ fm}^{-2}$ and $\beta_\alpha=0.375 \text{ fm}^{-2}$. \vec{r}_i is the coordinate of particle i in ${}^6\text{Li}$ relative to the centre of mass of ${}^6\text{Li}$. \vec{R}_d and \vec{R}_α represent the centre of mass for the corresponding clusters. N_d and N_α are the cor-

responding normalized factors. The calculated value of root-mean-square matter radius and that of charge radius are both 2.54 fm, which agree with the experimental value $2.54 \pm 0.03 \text{ fm}$ [43] (the measured values for these two radii are the same). The charge form factor of elastic electron scattering by ${}^6\text{Li}$ is also calculated, as shown in Fig. 2. Reasonable agreement is obtained with the experimental data [42].

B. The CDCC method and the sum-rule model

Detailed CDCC formalism can be found in Refs. [19, 27, 39, 44]. In this method, a finite number of discretized and square-integrable states are adopted to represent the continuum states of the projectile. Hence, the total wave function with total angular momentum J and parity π can be expressed as

$$\Psi^{J\pi} = \sum_{\beta} \Phi_{\beta}^{J\pi} \psi_{\beta} \quad (3)$$

where β represents the reaction channel. ψ_{β} is the internal wave function of ${}^6\text{Li}$ in β channel. The wave functions for bound and discretized states are expressed on the same footing. $\Phi_{\beta}^{J\pi}$ is the relative motion wave function between the ${}^6\text{Li}$ in β channel and target. $\Phi_{\beta}^{J\pi}$ is determined by the coupled-channel equations

$$[T + E_{\beta} - U_{\beta\beta}^{J\pi}] \Phi_{\beta}^{J\pi} = - \sum_{\beta' \neq \beta} U_{\beta\beta'}^{J\pi} \Phi_{\beta'}^{J\pi}, \quad (4)$$

where E_{β} is the channel energy. T denotes the kinetic energy of ${}^6\text{Li}$ -target relative motion. The coupling matrix element $U_{\beta\beta'}^{J\pi}$ is calculated as

$$U_{\beta\beta'}^{J\pi} = \langle \psi_{\beta} | U_{\alpha-T} + U_{d-T} | \psi_{\beta'} \rangle, \quad (5)$$

where $U_{\alpha-T}$ and U_{d-T} are the optical potentials for α and d with the target respectively. The imaginary parts of the optical potentials, $W_{\alpha-T}$ and W_{d-T} , are responsible for the absorption of ${}^6\text{Li}$ by the target. Therefore, the coupling matrix elements corresponding to the absorption is given by

$$W_{\beta\beta'}^{J\pi} = \langle \psi_{\beta} | W_{\alpha-T} + W_{d-T} | \psi_{\beta'} \rangle. \quad (6)$$

The total fusion cross section is then obtained as

$$\sigma_{TF} = \sum_{J=0}^{J_{\max}} \sigma_J, \quad (7)$$

where

$$\sigma_J = \frac{K}{E} \sum_{\pi\beta\beta'} \langle \Phi_{\beta}^{J\pi} | W_{\beta\beta'}^{J\pi} | \Phi_{\beta'}^{J\pi} \rangle. \quad (8)$$

K is the projectile-target relative wave number in the incident channel. It should be emphasized that the wave

functions of all channels, including open and closed channels, are required in the calculations for σ_J with Eq. (8). This method is equivalent to the computing approach with S matrix [45], in which only the S matrices of open channels are used.

According to the sum-rule model, the complete fusion cross section can be extracted directly as

$$\sigma_{CF} = \sum_{J=0}^{J_c} \sigma_J, \quad (9)$$

where J_c is the cut-off angular momentum (see Sec. IV B for details).

III. CONVERGENCE OF TOTAL FUSION CROSS SECTION CALCULATIONS

Optical potential with a short-range imaginary part can be applied to calculate the fusion cross section, which is equivalent to the use of an incoming boundary condition inside the Coulomb barrier [46]. In principle, the calculated fusion cross section should be independent of the imaginary part of the optical potential.

In this work, the São Paulo potential version 2 (SPP2) [47] is adopted for the real parts of the nuclear interactions between the α and d clusters with the target. SPP2 potential is calculated with the double folding method, which requires the nucleon distributions of projectile and target. We adopt the theoretical nuclear distribution embedded in the code for the target, which is calculated by an axially-symmetric self-consistent Dirac-Hartree-Bogoliubov mean field approach [48]. The nucleon distributions for α and d clusters are calculated with the wave function in Eq. (2). For the Coulomb potentials, the radius factor r_C for two clusters with the target are both set to be 1.5 fm.

The short-range imaginary parts of the d -target and α -target optical potentials are parameterized in the Woods-Saxon form. Their radius factor r_W and diffuseness parameter a_W are set to be 0.8 fm and 0.1 fm respectively so that the imaginary parts are inside the Coulomb barrier completely. The depths of the two imaginary parts W_0 are set to be the same, varying from 20.0 MeV to 80.0 MeV to examine the convergence of total fusion cross section calculation.

Following our previous study [27], the internal Hamiltonian of ${}^6\text{Li}$ is diagonalized by the regularized Lagrange-Laguerre mesh method [49–51]. This way of discretizing the continuum states is called the pseudo-state method, which diagonalizes the Hamiltonian by square integrable basis functions and can generate the bound and pseudo-states together. The pseudo-states are used to represent the continuum states. The basis functions are defined as

$$f_i(r) = \frac{(-1)^i L_N(r/h)}{\sqrt{hx_i}} r e^{-r/2h}, i = 1, 2, \dots, N, \quad (10)$$

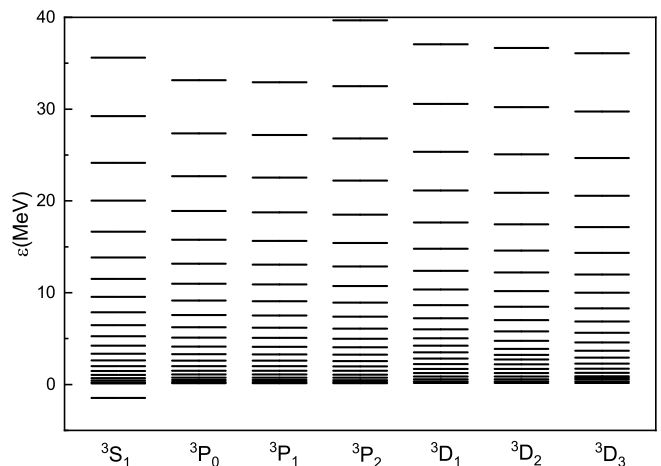


FIG. 3. Energy spectrum of ${}^6\text{Li}$ bound and pseudo-states up to D -wave continuum and 40.0 MeV, calculated with regularized Lagrange-Laguerre mesh method ($N=35$ and $h=0.5$ fm).

where L_N is the Laguerre polynomial of degree N . x_i corresponds to the zeros of L_N , that is

$$L_N(x_i) = 0, i = 1, 2, \dots, N. \quad (11)$$

h is a scaling parameter, adopted to the typical size of the system. For more details one can see Refs. [27, 49–51].

In this paper, the number of basis function N and the scaling parameter h are set to be 35 and 0.5 fm respectively. Many tests have been performed to ensure that the calculated fusion cross sections are insensitive to the parameters N and h . Fig. 3 shows the energy spectrum of ${}^6\text{Li}$ bound and pseudo-states up to D -wave continuum and 40.0 MeV.

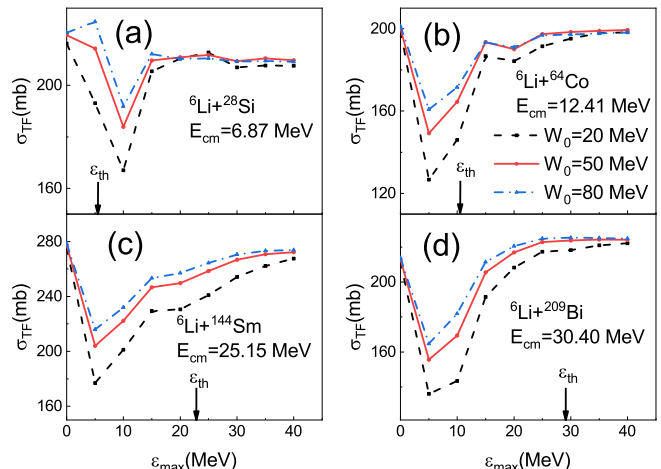


FIG. 4. (Color online) Calculated TF cross sections for ${}^6\text{Li}+{}^{28}\text{Si}$, ${}^{64}\text{Ni}$, ${}^{144}\text{Sm}$ and ${}^{209}\text{Bi}$ systems at $E_{cm} = V_B$ with different imaginary part depth W_0 and maximum energy of the continuum state ε_{max} . V_B represents the Coulomb barrier. The arrow indicates the threshold energy of the continuum states $\varepsilon_{th} = E_{c.m.} - 1.47$ MeV. See text for details.

We firstly perform calculations for ${}^6\text{Li}+{}^{28}\text{Si}$, ${}^{64}\text{Ni}$, ${}^{144}\text{Sm}$ and ${}^{209}\text{Bi}$ systems at incident energy in center of mass system $E_{cm} = V_B$, where V_B is the Coulomb barrier measured in the references. $V_B=6.87, 12.41, 25.15$ and 30.40 MeV for ${}^6\text{Li}+{}^{28}\text{Si}$ [15], ${}^{64}\text{Ni}$ [52], ${}^{144}\text{Sm}$ [8] and ${}^{209}\text{Bi}$ [17] systems respectively. $l=0, 1$ and 2 states are taken into CDCC calculations. The calculations are made with the maximum continuum energy ε_{max} from 0 to 40 MeV for all partial waves with the depth of the imaginary potential being $20, 50$ and 80 MeV, respectively. The results are shown in Fig. 4. From these results, we can get the following important information:

1. The maximum continuum energy set in the calculations ε_{max} should be large enough to ensure that the σ_{TF} do not depend on the choice of the imaginary potential depth. On the other hand, when ε_{max} is set large enough, the resulting σ_{TF} values do converge to a value which is independent of the depths of the imaginary potentials;
2. For ${}^6\text{Li}+{}^{28}\text{Si}$, ${}^{64}\text{Ni}$ and ${}^{144}\text{Sm}$ systems, the inclusion of closed channels is necessary for the convergence of the total fusion cross sections.
3. For ${}^6\text{Li}+{}^{209}\text{Bi}$ system, the σ_{TF} calculated with $\varepsilon_{max}=\varepsilon_{th}$ only differs from that calculated with $\varepsilon_{max}=40.0$ MeV by 0.3% when $W_0=50$ MeV. The coupling effect of closed channels is weak for ${}^6\text{Li}$ total fusion with such a heavy nucleus.

Practically, $\varepsilon_{max} = 40$ MeV seems to be sufficient for all the four reaction systems. In this case, the changes in the total fusion cross sections are less than 2% when the imaginary potential depth changes from 20 to 80 MeV. This ε_{max} is well above the threshold energy of the continuum state $\varepsilon_{th}=E_{c.m.} - 1.47$ MeV and the closed channels are well included in calculations.

For a further understanding of how the cut-off of continuum state energy and the imaginary part of optical potentials influence the fusion cross section calculations, we compare the radial relative wave function for ${}^6\text{Li}+{}^{64}\text{Ni}$ system at $E_{c.m.} = V_B$ with different ε_{max} and W_0 . The radial relative wave function is defined as

$$u_{\beta}^J(R) = R\Psi_{\beta}^J(R), \quad (12)$$

where R is the relative distance between the centers of mass of ${}^6\text{Li}$ and target. To explicate the wave functions, the orbital angular momentums of the projectile-target relative motive in incoming and outgoing channels are required, namely L and L' . The radial wave functions at $J^{\pi}=1^+, 4^-$ and 10^+ are calculated for comparison. The partial wave fusion cross section σ_J reaches a maximum at $J=4$, which is also the cut-off angular momentum for this reaction (See Sec. IV B for more details).

In the present work, we study the influence of ε_{max} and W_0 on wave functions of elastic scattering, 3^+ resonance breakup and closed channels. The 3^+ resonance state of ${}^6\text{Li}$ is represented by the pseudo-state in 3D_3 partial wave

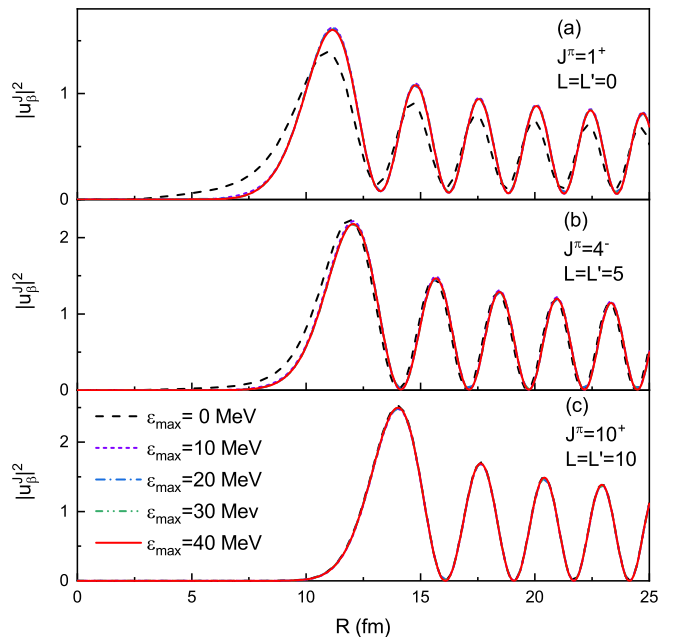


FIG. 5. (Color online) Square of the absolute value of the radial wave functions, $|u_{\beta}^J|^2$, of elastic scattering channel for ${}^6\text{Li}+{}^{64}\text{Ni}$ reaction at $E_{c.m.} = V_B = 12.41$ MeV. The wave functions calculated with $\varepsilon_{max}=0, 10, 20, 30$ and 40 MeV are represented by dashed, short dashed, dash-dotted, dash-double-dotted and solid lines respectively. The subfigures (a), (b) and (c) show the $|u_{\beta}^J|^2$ at $J^{\pi}=1^+, 4^-$ and 10^+ with $L=L'=0, 5$ and 10 respectively. See text for details.

with eigen energy 0.7111 MeV. For the closed channel wave functions, the u_{β}^J of the pseudo-state in 3S_1 partial wave with eigen energy 11.5108 MeV are calculated.

As the wave functions are used to calculate fusion cross sections as shown in Eq. (8), we focus on the square of the absolute value of wave functions $|u_{\beta}^J|^2$. With a fixed $W_0=50$ MeV, the wave functions are calculated with $\varepsilon_{max}=0, 10, 20, 30$ and 40 MeV. Fig. 5 shows $|u_{\beta}^J|^2$ of elastic scattering. $L=L'=0, 5$ and 10 for $J^{\pi}=1^+, 4^-$ and 10^+ respectively. It is observed that $|u_{\beta}^J|^2$ well converges with $\varepsilon_{max}=10$ MeV, which coincides with the general adopted ε_{max} for obtaining converged ${}^6\text{Li}$ elastic scattering angular distributions.

The $|u_{\beta}^J|^2$ for 3^+ resonance breakup are plotted in Fig. 6 for comparison. $L=0, 5$ and $10, L'=2, 7$ and 8 for $J^{\pi}=1^+, 4^-$ and 10^+ respectively. Different from the elastic scattering, the convergence of $|u_{\beta}^J|^2$ for 3^+ resonance breakup needs a pretty high $\varepsilon_{max}=40$ MeV, especially in the inner region ($R < 15$ fm).

In Fig. 7, the $|u_{\beta}^J|^2$ of the closed channels are shown. Although the wave functions are not completely converged with $\varepsilon_{max}=40$ MeV, we found that these small differences between the closed channel wave functions calculated with $\varepsilon_{max}=30$ and 40 MeV have little effect on the fusion cross sections.

In Eq. (8), the partial wave fusion cross section are

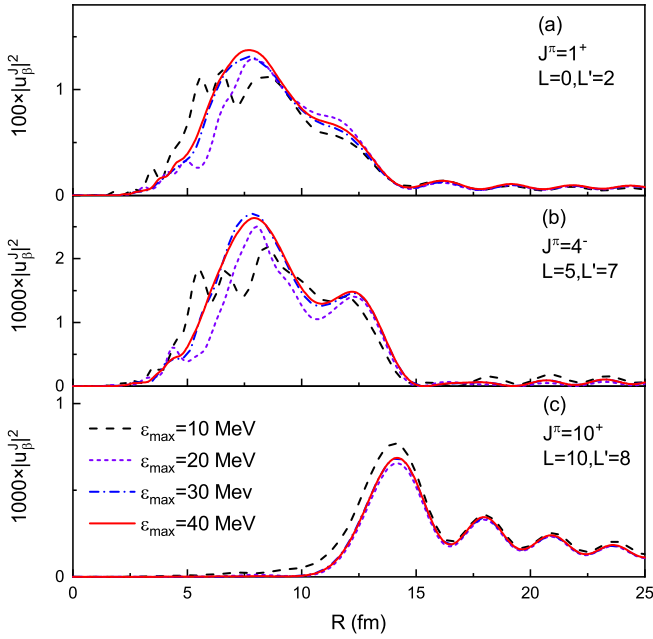


FIG. 6. (Color online) Same as Fig. 5 but for 3^+ resonance breakup. The wave functions calculated with $\varepsilon_{max}=10, 20, 30$ and 40 MeV are denoted by dashed, short dashed, dash-dotted and solid lines respectively. $L=0, 5$ and $10, L'=2, 7$ and 8 for $J^\pi=1^+, 4^-$ and 10^+ respectively. The $|u_\beta^J|^2$ in subfigures (a), (b) and (c) are multiplied by $100, 1000$ and 1000 respectively.

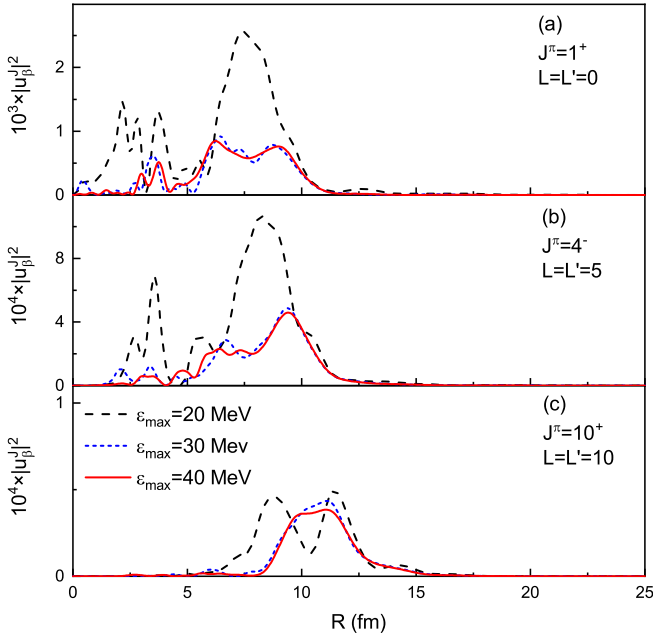


FIG. 7. (Color online) Same as Fig. 5 but for the closed channel. The wave functions calculated with $\varepsilon_{max}=20, 30$ and 40 MeV are denoted by dashed, short dashed and solid lines respectively. $L=L'=0, 5$ and 10 for $J^\pi=1^+, 4^-$ and 10^+ respectively. The $|u_\beta^J|^2$ in subfigures (a), (b) and (c) are multiplied by $10^3, 10^4$ and 10^4 respectively.

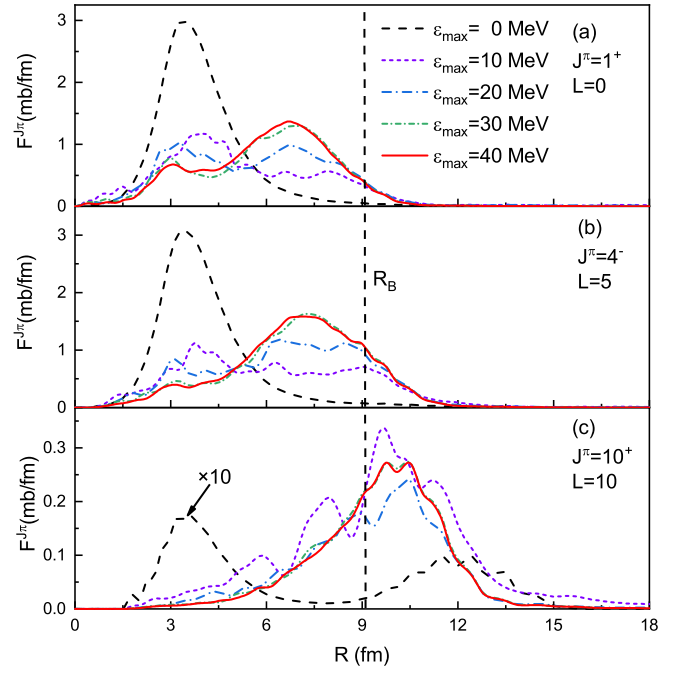


FIG. 8. (Color online) The integrands F for ${}^6\text{Li}+{}^{64}\text{Ni}$ reaction at $E_{c.m.} = V_B = 12.41$ MeV. The integrands calculated with $\varepsilon_{max}=0, 10, 20, 30$ and 40 MeV are denoted by dashed, short dashed, dash-dotted, short dash-dotted and solid lines respectively. They are evaluated at (a) $J^\pi=1^+, L=0$, (b) $J^\pi=4^-, L=5$ and (c) $J^\pi=10^+, L=10$. $R_B=9.1$ fm is the Coulomb barrier radius [52]. The F calculated with $\varepsilon_{max}=0$ at $J^\pi=10^+$ is multiplied by 10 for easier viewing.

calculated in an integration method. We define

$$F^{J^\pi}(R) = \frac{K}{E} \sum_{\beta\beta'} \Phi_\beta^{J^\pi*}(R) W_{\beta\beta'}^{J^\pi}(R) \Phi_{\beta'}^{J^\pi}(R). \quad (13)$$

Therefore

$$\sigma_J = \sum_\pi \int F^{J^\pi}(R) dR. \quad (14)$$

One point worth emphasizing is that F^{J^π} is dependent on J, π and L . The summation of L is necessary for the projectile with non-zero spin in the calculation of σ_J , but we omit it in Eq. (14) for simplification. As the range of $W_{\beta\beta'}^{J^\pi}$ is no more than 15 fm in general, it can be deduced that F is sensitive to the wave functions in the inner part and the convergence of F also requires a high ε_{max} .

The F^{J^π} at $J^\pi=1^+, 4^-$ and 10^+ are plotted in Fig. 8 with $L=0, 5$ and 10 respectively. Convergence within the deviation of less than 2% is reached with $\varepsilon_{max}=40$ MeV. The F^{J^π} calculated with $\varepsilon_{max}=0$ and 40 MeV have the same order of magnitude at $J^\pi=1^+$ and 4^- , but the former becomes about 10 times less than the latter at $J^\pi=10^+$. We multiply the F^{J^π} calculated with $\varepsilon_{max}=0$ at $J^\pi=10^+$ by 10 for easier viewing. A more detailed discussion about the influence of ε_{max} on σ_J will be given in Sec. IV B. On the other hand, the maximum of F^{J^π}

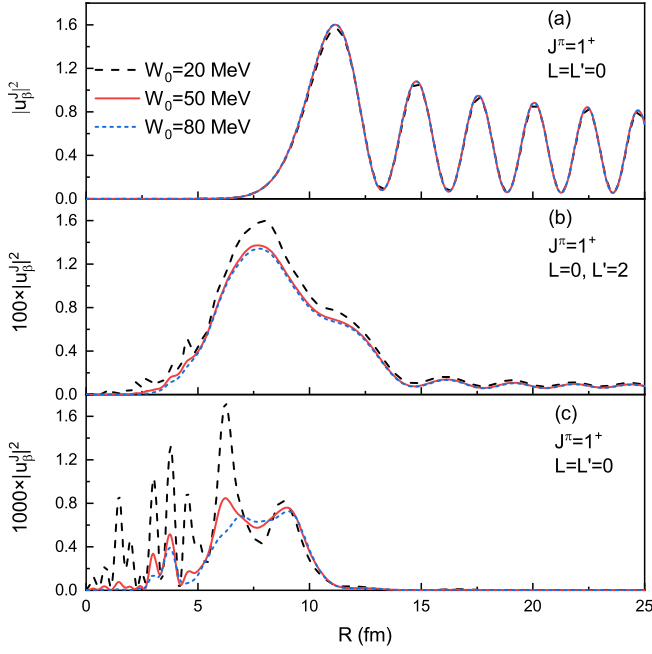


FIG. 9. (Color online) Square of the absolute value of the radial wave functions, $|u_\beta^J|^2$, for ${}^6\text{Li}+{}^{64}\text{Ni}$ reaction at $E_{c.m.} = V_B = 12.41$ MeV and $J^\pi=1^+$. The wave functions calculated with $W_0=20, 50$ and 80 MeV are represented by dashed, solid, and short dashed lines respectively. The sub-figures (a), (b) and (c) show the $|u_\beta^J|^2$ of elastic scattering, 3^+ resonance breakup and closed channel respectively. The $|u_\beta^J|^2$ of 3^+ resonance breakup and closed channel are multiplied by 100 and 1000 respectively. See text for details.

locates at $R=3.4$ fm when $\varepsilon_{max}=0$ and it moves outwards with the increase of ε_{max} . The peak of converged F^{J^π} at $J^\pi=10^+$ even locates outside of the Coulomb barrier radius $R_B=9.1$ fm [52]. The above comparisons indicate that the continuum coupling effect not only increases the partial wave fusion cross sections at relatively higher partial waves but also fully changes the fusion mechanism.

Another worth-considering issue is that the total fusion cross section is independent of the imaginary part of optical potentials when ε_{max} is large enough. With a fixed $\varepsilon_{max}=40$ MeV, we investigate how the u_β^J changes as the potential depth of the imaginary part varies. Fig. 9 shows the $|u_\beta^J|^2$ calculated with $W_0=20, 50$ and 80 MeV at $J^\pi=1^+$. As W_0 increases from 20 to 80 MeV, the $|u_\beta^J|^2$ of elastic scattering have hardly any changes, while the $|u_\beta^J|^2$ of 3^+ resonance breakup and closed channel vary visibly and their values are negatively correlated with W_0 in the very inner regions $R < 4$ and 7 fm respectively. For example, the $|u_\beta^J|^2$ of closed channel calculated with $W_0=20, 50$ and 80 MeV all reach a peak at $R=3.75$ fm and their values are 0.0013, 0.0005 and 0.0003 respectively.

Comparisons at $J^\pi=4^-$ and 10^+ are presented in Figs. 10 and 11. The $|u_\beta^J|^2$ of elastic scattering is stable against W_0 . The value of $|u_\beta^J|^2$ of 3^+ resonance breakup is still

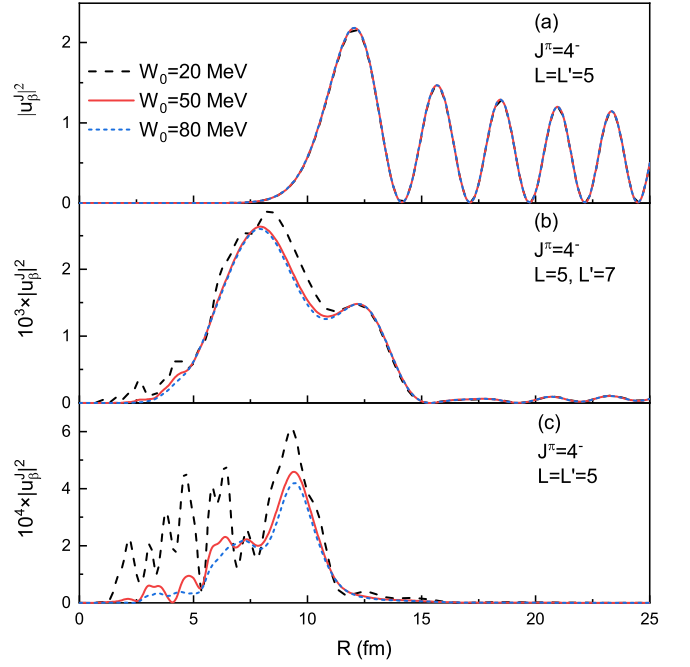


FIG. 10. (Color online) Same as Fig. 9 but for $J^\pi=4^-$. The $|u_\beta^J|^2$ of 3^+ resonance breakup and closed channel are multiplied by 10^3 and 10^4 respectively.

negatively correlated with W_0 at $J^\pi=4^-$ in the region $R < 4$ fm, but it becomes independent of W_0 at $J^\pi=10^+$. However, for the $|u_\beta^J|^2$ of closed channel, the negative correlation with W_0 is kept at both $J^\pi=4^-$ and 10^+ .

Fig. 12 shows the integrands F^{J^π} calculated with $W_0=20, 50$ and 80 MeV at $J^\pi=1^+, 4^-$ and 10^+ . The F^{J^π} calculated with $W_0=20$ MeV is flatter than those calculated with $W_0=50$ and 80 MeV. Fortunately, although the three kinds of F do not coincide perfectly, their integrations are almost the same, which will not affect the subsequent analysis. Furthermore, an overall comparison of partial wave fusion cross sections calculated with different W_0 is presented in Fig. 13. σ_J at each J is indeed independent of W_0 when $\varepsilon_{max}=40$ MeV.

In Fig. 14, an example of the convergence of TF cross sections calculations is shown for the ${}^6\text{Li}+{}^{64}\text{Ni}$ system at energies around the Coulomb barrier. In these calculations, $W_0=50.0$ MeV. The CDCC calculations with $\varepsilon_{max}=40.0$ and 45.0 MeV are almost the same when $l=0, 1$ and 2 states are included. The inclusion of the states with higher l has an invisible effect on TF cross sections. Therefore, the convergence of TF cross section calculations in the present work is ensured.

IV. CALCULATED RESULTS AND ANALYSIS

In this section, we study the continuum coupling effect on total and complete fusion. The CDCC calculations are performed with $W_0=50.0$ MeV and $l=0, 1$ and 2 con-

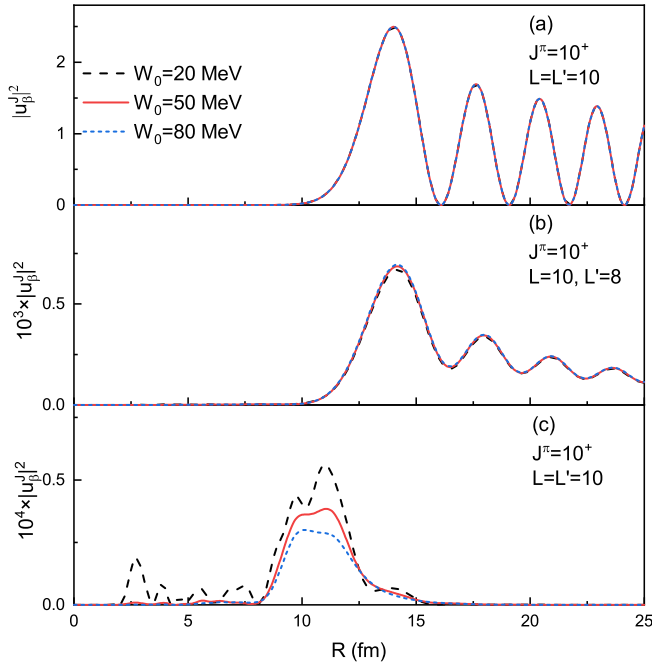


FIG. 11. (Color online) Same as Fig. 9 but for $J^\pi=10^+$. The $|u_\beta^j|^2$ of 3^+ resonance breakup and closed channel are multiplied by 10^3 and 10^4 respectively.

tinuum states. Four types of calculations are performed:

- (1) No continuum states are included, i.e., single channel calculations;
- (2) Continuum states below $\varepsilon_{max}=6.0$ MeV are included, which include the resonance states;
- (3) Continuum states below $\varepsilon_{max}=\varepsilon_{th}$ are included, closed channels are ignored;
- (4) Continuum states below $\varepsilon_{max}=40.0$ MeV are included.

It should be emphasised that the second type of calculation is not made for ${}^6\text{Li}+{}^{28}\text{Si}$ system at some low incident energies to avoid the inclusion of closed channels. The fourth type of calculation is not performed for ${}^6\text{Li}+{}^{209}\text{Bi}$ system at a few high energies, where ε_{th} is larger than 40.0 MeV.

Although the second and third types of calculations can not provide converged TF cross sections, they can be applied to analyse the coupling effect of the continuum states in different energy regions. In the present work, we mainly focus on the coupling effect from the continuum states above the resonance energy regions ($\varepsilon \geq 6.0$ MeV). The coupling effects of open and closed channels can be distinguished by comparing the results of the third and fourth types of calculations.

A. Continuum coupling effect on total fusion

Figures 15 and 16 show the calculated TF cross sections for ${}^6\text{Li}+{}^{28}\text{Si}$, ${}^{64}\text{Ni}$, ${}^{144}\text{Sm}$ and ${}^{209}\text{Bi}$ systems, and their comparison with the experimental data [7, 8, 15,

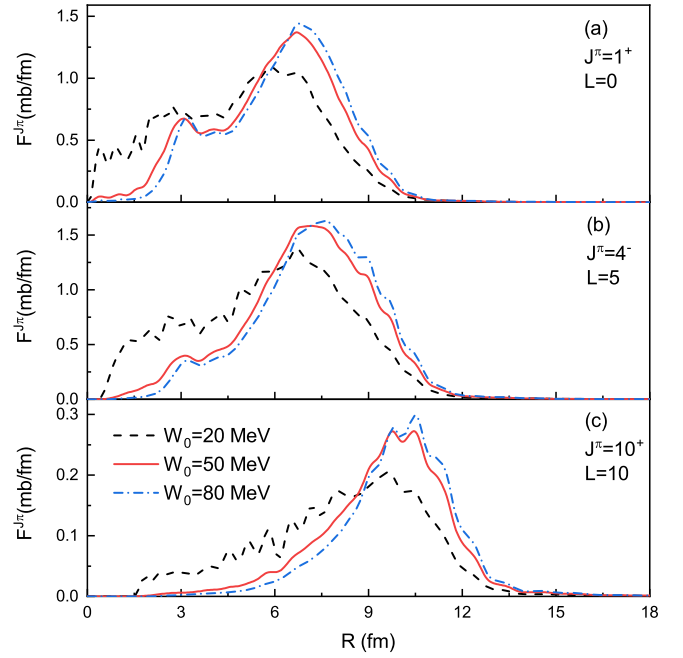


FIG. 12. (Color online) The integrands F for ${}^6\text{Li}+{}^{64}\text{Ni}$ reaction at $E_{c.m.} = V_B = 12.41$ MeV. The integrands calculated with $W_0=20, 50$ and 80 MeV are denoted by dashed, solid and dash-dotted lines respectively. See text for details.

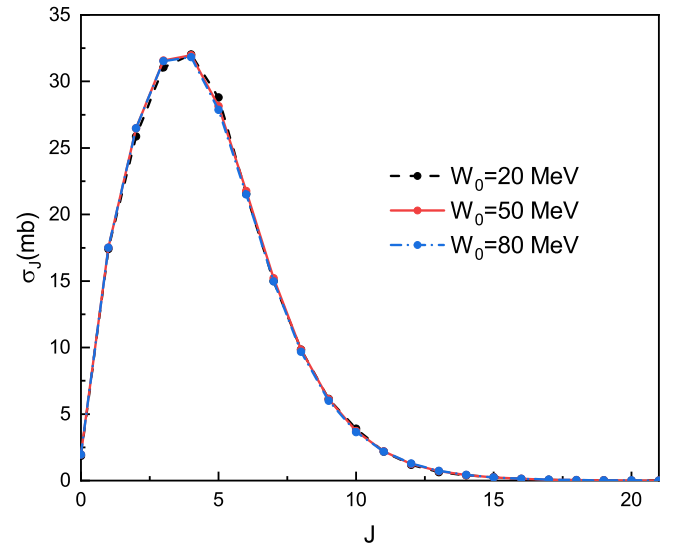


FIG. 13. (Color online) The partial wave fusion cross section σ_J for ${}^6\text{Li}+{}^{64}\text{Ni}$ reaction at $E_{c.m.} = V_B = 12.41$ MeV. The σ_J with $W_0=20, 50$ and 80 MeV are denoted by dashed, solid and dash-dotted lines respectively. See text for details.

17, 52–56]. The two figures are shown in logarithmic and linear scale, convenient to see the TF cross sections at energies below and above the Coulomb barrier respectively.

In general, the agreement between the converged CDCC results and the measured value is reasonably good in the sub-barrier region, but the converged CDCC

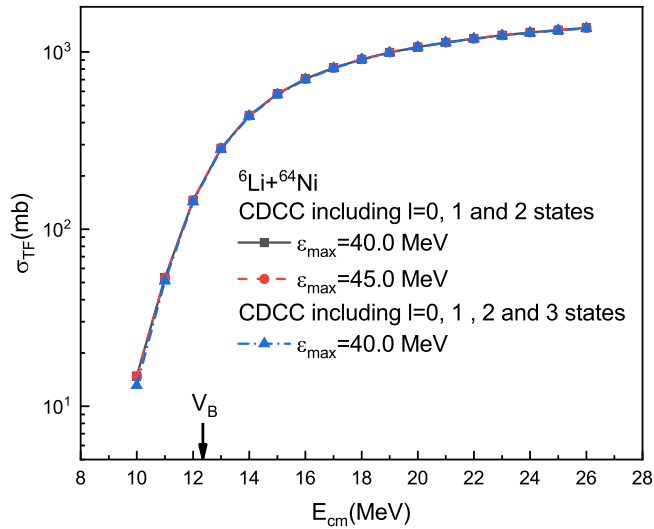


FIG. 14. (Color online) Calculated TF cross sections for ${}^6\text{Li}+{}^{64}\text{Ni}$ system with different conditions. The arrow indicates the Coulomb barrier. See text for details.

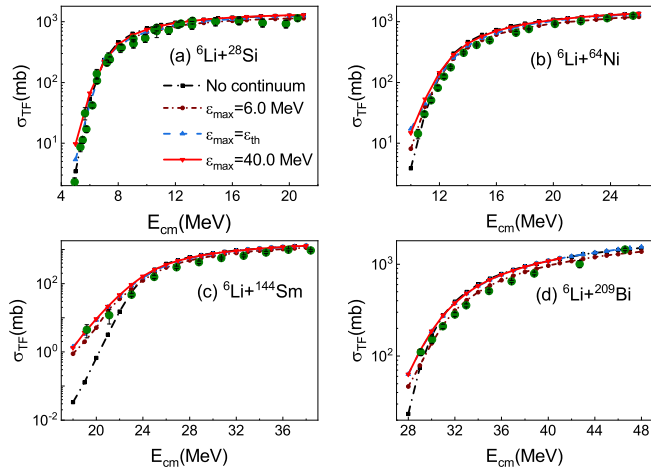


FIG. 15. (Color online) Calculated TF cross sections for ${}^6\text{Li}+{}^{28}\text{Si}$, ${}^{64}\text{Ni}$, ${}^{144}\text{Sm}$ and ${}^{209}\text{Bi}$ systems shown in logarithmic scale. Experimental data are taken from Refs. [7, 8, 15, 17, 52–56]. See text for details.

results overestimate the experimental data at energies above the Coulomb barrier for ${}^{64}\text{Ni}$, ${}^{144}\text{Sm}$ and ${}^{209}\text{Bi}$ targets. This overestimation may be resulted by the following reasons:

(1) The adopted nuclear potentials for α and d with targets (SPP2) are the systematic research results for various elastic scattering experimental data and it is expected that there are some disagreements for specific reaction systems.

(2) In the present work, only the ${}^6\text{Li} \rightarrow \alpha + d$ channel is taken into account. However, there are other important reaction channels, such as n -transfer, which can influence the TF cross sections.

(3) Rath et al. [56] measured the incomplete fusion

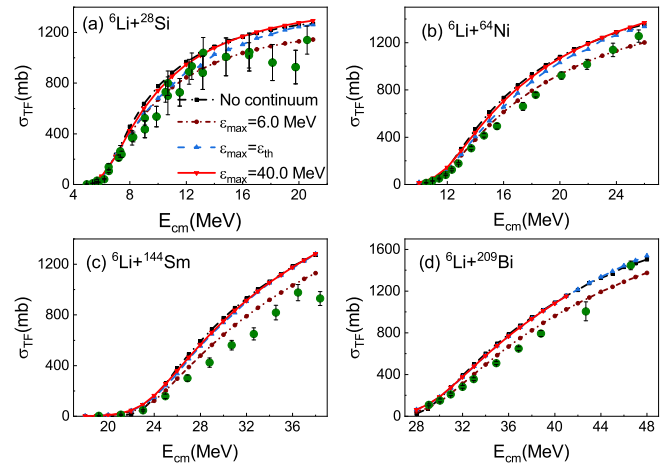


FIG. 16. (Color online) Same as Fig. 15 but shown in linear scale.

cross section for ${}^6\text{Li}+{}^{144}\text{Sm}$ by summing the detected cross sections for d - and α -capture, in which not all possible evaporation residue channels were included. Therefore, the values of the ICF and TF(=CF+ICF) can be considered as the lower limit. Similarly, Dasgupta et al. [7, 17] measured the fusion cross sections for ${}^6\text{Li}+{}^{209}\text{Bi}$ system by detecting α particles emitted by the evaporation residues of the compound nuclei. However, they missed the contribution from ${}^{209}\text{Po}$, which could not be measured due to its long half-life (about 200 yr). According to the statistical model estimation [7], the contribution from ${}^{209}\text{Po}$ was expected to be significant at the high energies.

For all the four collision systems, it can be seen in Figs. 15 and 16 that the results of the CDCC calculations become close to the single channel results in the above-barrier region by varying ϵ_{max} from 6.0 MeV to 40.0 MeV. In the sub-barrier region, the calculated TF cross sections are enhanced by increasing ϵ_{max} . To determine the continuum coupling effect on TF cross section, we define

$$\Gamma_i = \frac{\sigma_{TF}(i)}{\sigma_{TF}(1)} - 1, i = 2, 3, 4. \quad (15)$$

The $\sigma_{TF}(i)$ ($i = 1, 2, 3, 4$) denotes the TF cross section obtained by the i -th type of calculation as listed in the beginning of Sec. IV.

Fig. 17 presents the Γ_i -values ($i=2, 3$ and 4) for ${}^6\text{Li}+{}^{28}\text{Si}$, ${}^{64}\text{Ni}$, ${}^{144}\text{Sm}$ and ${}^{209}\text{Bi}$ systems. Compared with the TF cross sections obtained without continuum states coupling, there is a 10-15% suppression at energies above the Coulomb barrier for these reaction systems when $\epsilon_{max}=6.0$ MeV (See the results of Γ_2). However, this suppression is much reduced for ${}^6\text{Li}+{}^{28}\text{Si}$ and eliminated for ${}^6\text{Li}+{}^{64}\text{Ni}$, ${}^{144}\text{Sm}$ and ${}^{209}\text{Bi}$ when the converged result is obtained with $\epsilon_{max}=40.0$ MeV (See the results of Γ_4). In the sub-barrier region, the theoretical TF cross sections are further enhanced by increasing ϵ_{max} . A detailed discussion is given below.

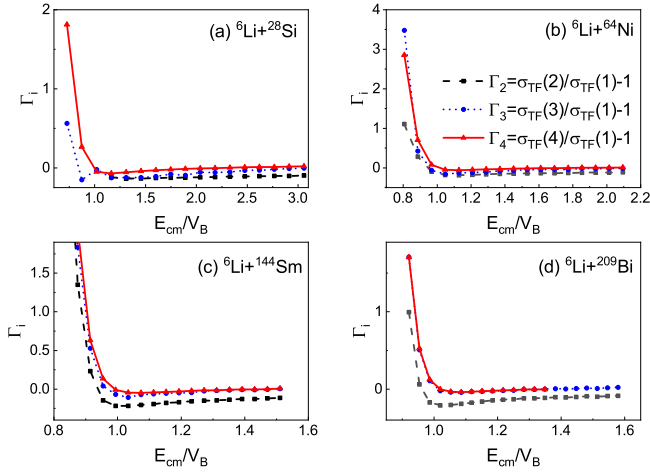


FIG. 17. (Color online) Γ_i ($i=2, 3$ and 4) for ${}^6\text{Li}+{}^{28}\text{Si}$, ${}^{64}\text{Ni}$, ${}^{144}\text{Sm}$ and ${}^{209}\text{Bi}$ systems.

For the ${}^6\text{Li}+{}^{28}\text{Si}$ system, with the ε_{max} increasing from 6.0 MeV to ε_{th} , the suppression remains nearly unchanged in the region $1.0 \leq E_{cm}/V_B \leq 1.8$ and is moderately reduced in $1.8 \leq E_{cm}/V_B \leq 2.5$ (See the results of Γ_3). Only when the closed channels are taken into CDCC calculations can the suppression effect be negligible. In higher incident energies, the TF cross sections obtained with $\varepsilon_{max}=\varepsilon_{th}$ and 40.0 MeV are almost the same, indicating that the coupling effect of closed channels can be ignored in this high energy region. In the sub-barrier region, a much stronger enhancement is provided by the calculation with $\varepsilon_{max}=40.0$ MeV, where the coupling effect of closed channels is completely taken into account.

For the medium mass targets ${}^{64}\text{Ni}$ and ${}^{144}\text{Sm}$, the calculated results obtained with $\varepsilon_{max}=\varepsilon_{th}$ are slightly smaller than the single channel results in a very narrow region around E_{cm} . But the converged CDCC calculation, which includes the closed channels, has only an enhanced effect on σ_{TF} at energies below the Coulomb barrier. When $E_{cm} > 1.1 V_B$, the values obtained with $\varepsilon_{max}=\varepsilon_{th}$ and 40.0 MeV are almost the same as the single channel results. In the energy region $E_{cm} < 0.9 V_B$, the CDCC calculations with $\varepsilon_{max}=\varepsilon_{th}$ and 40.0 MeV provide a similar enhancement effect on TF cross section, which is stronger than that given by the calculation with $\varepsilon_{max}=6.0$ MeV.

As the Coulomb barrier for ${}^6\text{Li}+{}^{209}\text{Bi}$ system is quite high, the results obtained with $\varepsilon_{max}=40.0$ MeV are almost the same as those obtained with $\varepsilon_{max}=\varepsilon_{th}$. Their results are approximately equal to the results obtained without continuum states coupling at energies above the Coulomb barrier. In the sub-barrier region, the TF cross sections are further enhanced by taking higher energy continuum states ($\varepsilon \geq 6.0$ MeV) into CDCC calculations.

The above results seem to suggest that the coupling effects from low-energy continuum states ($0 \leq \varepsilon \leq 6.0$ MeV) and higher-energy continuum states ($6.0 \leq \varepsilon \leq 40.0$ MeV) add destructively for the total fusion cross

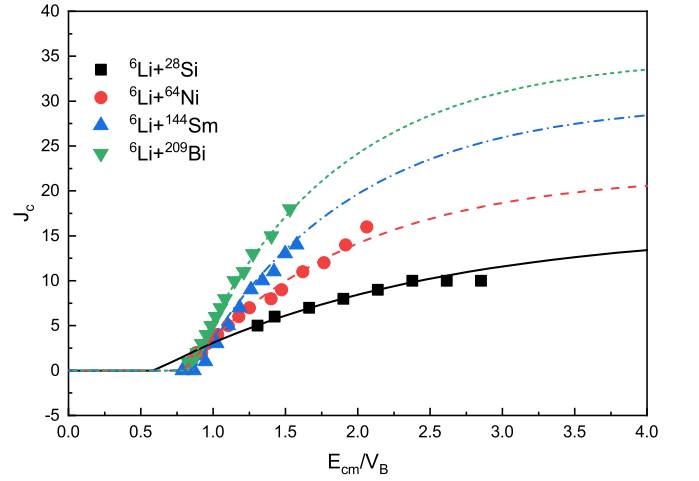


FIG. 18. (Color online) The extracted cut-off angular momentum J_c for ${}^6\text{Li}+{}^{28}\text{Si}$ (squares), ${}^{64}\text{Ni}$ (circles), ${}^{144}\text{Sm}$ (upper triangular) and ${}^{209}\text{Bi}$ (lower triangular) systems. The corresponding fitting curves are represented by the solid, dashed, dashed-dotted and short-dashed lines respectively.

TABLE III. The values of C_0 , C_1 and J_{crit} .

system	C_0	C_1	J_{crit}
${}^6\text{Li}+{}^{28}\text{Si}$	0.54	0.60	16
${}^6\text{Li}+{}^{64}\text{Ni}$	0.86	0.80	22
${}^6\text{Li}+{}^{144}\text{Sm}$	0.94	0.86	30
${}^6\text{Li}+{}^{209}\text{Bi}$	1.00	0.82	35

sections at energies above the Coulomb barrier. In the end, the converged CDCC results provide nearly the same total fusion reactions as single-channel calculations. This is an interesting observation.

B. Continuum coupling effect on complete fusion

Based on the converged TF cross sections and the experimental data for complete fusion [7, 8, 15, 17, 52, 56], we apply the sum-rule model to extract the cut-off angular momentum J_c and CF cross section σ_{CF} , as shown in Eq. (9).

In the early researches [28–30], the sum-rule model was applied to the reactions at incident energies well above the Coulomb barrier. In these cases, CF and ICF processes can be well separated by a critical angular momentum, J_{crit} , which is nearly independent of the incident energy. Recently, Mukeru et al. combined this model with CDCC method to study the fusion of weakly bound nuclei at energies around the Coulomb barrier, such as ${}^8\text{Li}+{}^{208}\text{Pb}$ [31] and ${}^9\text{Be}+{}^{124}\text{Sn}$, ${}^{144}\text{Sm}$ and ${}^{208}\text{Pb}$ [32]. The angular momentum to separate the CF and ICF processes, J_c , was found to be incident-energy-dependent.

Following the method of Mukeru et al. [31, 32], J_c can

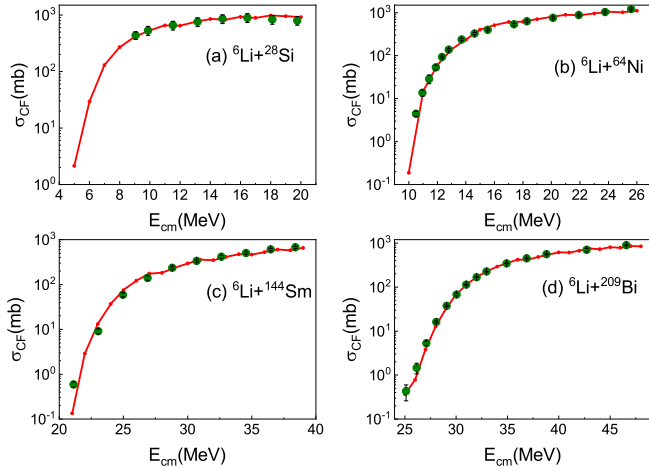


FIG. 19. (Color online) The CF cross sections extracted through the sum-rule model for ${}^6\text{Li}+{}^{28}\text{Si}$, ${}^{64}\text{Ni}$, ${}^{144}\text{Sm}$ and ${}^{209}\text{Bi}$ systems, compared with the experimental data [7, 8, 15, 17, 52, 56].

be linked to the critical angular momentum J_{crit} with an analytical expression

$$J_c = \left\{ 1 - \exp \left[-C_0 \left(\frac{E_{cm}}{V_B} - C_1 \right) \right] \right\} J_{crit}. \quad (16)$$

J_{crit} is calculated with the formalism in Ref. [28]. C_0 and C_1 are obtained by fitting J_c . Their values are listed in Table III. The extracted J_c and the fitting curves are plotted in Fig. 18. The fitted value is set to 0 when it is negative. As the energy decreases, it can be seen obviously that the fitting curve for ${}^6\text{Li}+{}^{28}\text{Si}$ returns to zero at $E_{cm}/V_B \approx 0.6$ while those for other systems return to 0 at $E_{cm}/V_B \approx 0.8$. As there is no available CF data for ${}^6\text{Li}+{}^{28}\text{Si}$ system in the sub-barrier energy region, this difference is expected to be explained with further experimental and theoretical studies.

The calculated CF cross sections are compared with experimental data in Fig. 19. Good agreement is obtained between theory and experiment. To analyse the continuum coupling effect on CF process, we pay close attention to the partial wave fusion cross sections σ_J in the partial waves below the cut-off angular momentum J_c , at energies below, near, above and well above the Coulomb barrier. In addition, it is practical to apply J_c for the single channel calculation to extract the cross section σ_{CF}^{1ch} , which can be regarded as the CF cross section without continuum coupling. It can be compared with σ_{CF} to determine the continuum effect on complete fusion quantitatively.

Fig. 20 shows the partial wave fusion cross sections σ_J for ${}^6\text{Li}+{}^{28}\text{Si}$ system at $E_{cm}=5.0, 7.0, 9.0$ and 12.0 MeV. At the first energy point which is below the Coulomb barrier, the σ_J of the single-channel calculation and the CDCC calculation with $\varepsilon_{max}=\varepsilon_{th}$ at $J \leq J_c$ are almost the same. It suggests that in this case, the continuum states of open channels have little coupling effect on com-

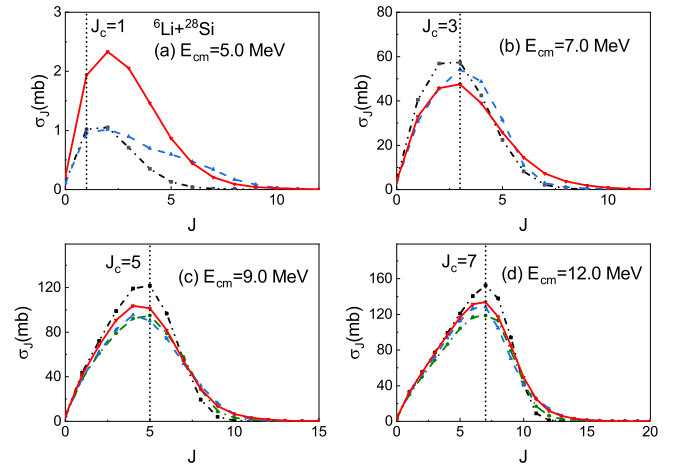


FIG. 20. (Color online) Partial wave fusion cross section σ_J for ${}^6\text{Li}+{}^{28}\text{Si}$ at $E_{cm}=5.0, 7.0, 9.0$ and 12.0 MeV. The four energy points correspond to the energies below, near, above and well above the Coulomb barrier respectively. The calculated results without continuum coupling and those with $\varepsilon_{max}=6.0$ MeV, ε_{th} and 40.0 MeV are plotted in black dashed-dotted, green dashed-dotted, blue dashed and red solid lines respectively. The short dotted lines represent the cut-off angular momentum J_c .

plete fusion, although the 3^+ and 2^+ resonance states have been taken into account. Only when the closed channels are taken into calculations will the σ_J in lower angular momenta be significantly enhanced. At $E_{cm}=9.0$ and 12.0 MeV, the converged σ_J in $J \leq J_c$ is slightly larger than those calculated with $\varepsilon_{max}=6.0$ MeV and ε_{th} . But they are all visibly smaller than the single channel results in $J_c - 2 \leq J \leq J_c$. Because of the continuum coupling, the σ_{CF} in the above-barrier region is smaller than σ_{CF}^{1ch} about 5-20%, which is consistent with the suppression factor of 15% given by Mandira and Lubian [15].

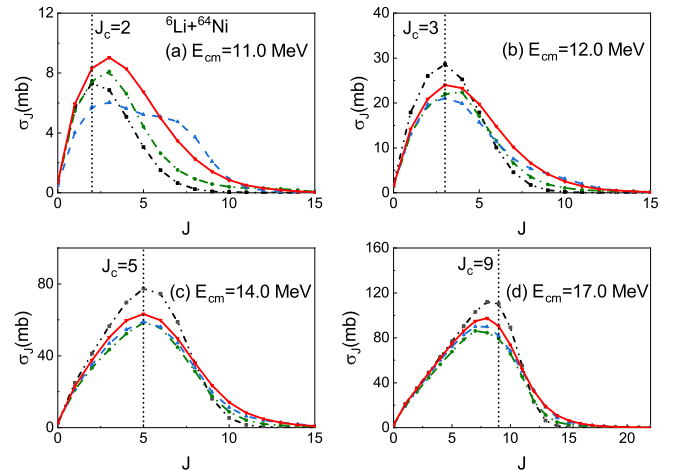


FIG. 21. (Color online) Same as Fig. 20 but for ${}^6\text{Li}+{}^{64}\text{Ni}$ at $E_{cm}=11.0, 12.0, 14.0$ and 17.0 MeV.

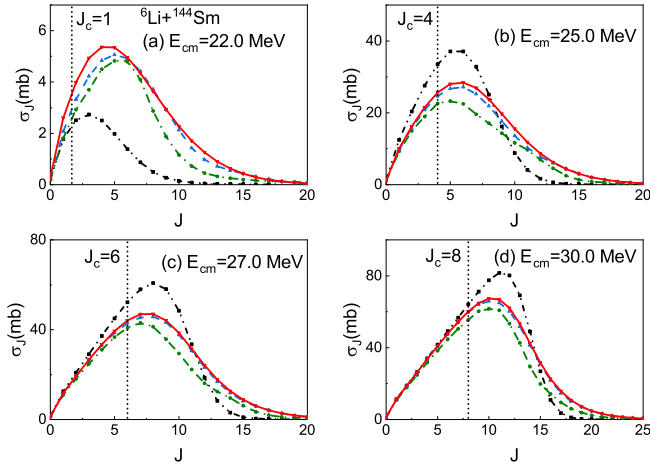


FIG. 22. (Color online) Same as Fig. 20 but for ${}^6\text{Li}+{}^{144}\text{Sm}$ at $E_{cm}=22.0, 25.0, 27.0$ and 30.0 MeV.

The partial wave fusion cross sections for ${}^6\text{Li}+{}^{64}\text{Ni}$ system are presented in Fig. 21. There is a noticeable issue shown in Fig. 21(a). At the energy (11.0 MeV) below the Coulomb barrier, the CDCC calculated σ_J in $J \leq J_c$ decreases firstly when ε_{max} increases from 6.0 MeV to ε_{th} and it then increases by including closed channels. Eventually, the converged σ_J is slightly larger than the single channel result in $J \leq J_c$. As the σ_J in $J \leq J_c$ obtained with the single channel calculation and the CDCC calculation with $\varepsilon_{max}=6.0$ MeV are almost the same, it can be concluded that the enhancement on σ_{CF} mainly comes from the continuum states above 6.0 MeV and the closed channels have a fundamental coupling effect. At $E_{cm}=12.0, 14.0$ and 17.0 MeV, the σ_J in $J \leq J_c$ obtained with $\varepsilon_{max}=40.0$ MeV are moderately larger than the results of other two kinds of CDCC calculations, while they are all smaller than the single channel result in $J_c - 2 \leq J \leq J_c$ observably. By comparing σ_{CF}^{1ch} and σ_{CF} , a 13-18% suppression factor is given at energies above the Coulomb barrier, in good agreement with the result of $13 \pm 7\%$ in Ref. [52].

In Fig. 22, the partial wave fusion cross sections σ_J for ${}^6\text{Li}+{}^{144}\text{Sm}$ system are plotted at $E_{cm}=22.0, 25.0, 27.0$ and 30.0 MeV. As ε_{max} increases from 6.0 MeV to 40.0 MeV, the σ_J in $J \leq J_c$ is slightly enlarged for all four energy points. The σ_{CF} is larger than the σ_{CF}^{1ch} at $E_{cm}=22.0$, while it becomes smaller about 5-25% at other three energies because of the reduction of σ_J in $J_c - 2 \leq J \leq J_c$. It is reasonably consistent with the suppression of $32 \pm 5\%$ in Ref. [8].

The partial wave fusion cross sections σ_J for ${}^6\text{Li}+{}^{209}\text{Bi}$ are presented in Fig. 23 at $E_{cm}=28.0, 30.0, 32.0$ and 35.0 MeV. The results obtained with $\varepsilon_{max}=\varepsilon_{th}$ and 40.0 MeV are almost the same in all partial waves, suggesting that the closed channels have hardly any coupling effect on this reaction system. On the other hand, the σ_J in $J \leq J_c$ is visibly enlarged at $E_{cm}=28.0$ and 30.0 MeV by increasing ε_{max} from 6.0 MeV to ε_{th} , showing the ob-

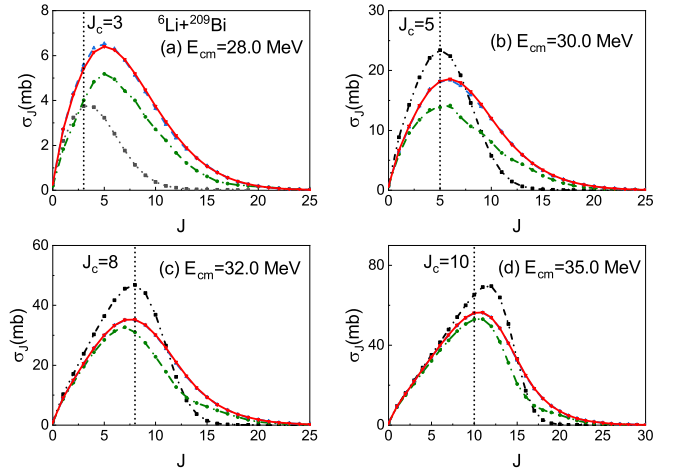


FIG. 23. (Color online) Same as Fig. 20 but for ${}^6\text{Li}+{}^{209}\text{Bi}$ at $E_{cm}=28.0, 30.0, 32.0$ and 35.0 MeV.

vious coupling effect of the continuum states above the resonance energy region. With the same improvement of ε_{max} , there is a slight enhancement on σ_J in $J \leq J_c$ at $E_{cm}=32.0$ and 35.0 MeV. Similarly with other reaction systems, σ_{CF} is higher than σ_{CF}^{1ch} at $E_{cm}=28.0$ MeV but becomes lower about 10-35% at higher energies, which agrees with the suppression of $36 \pm 3\%$ provided by Dasgupta et al. [7].

In addition, for all four reaction systems, we found that:

(1) At energies below the Coulomb barrier, the σ_J obtained by the converged CDCC calculation is larger than that obtained by single channel calculation at each J . Based on the sum-rule model, it indicates that continuum coupling increases both the complete fusion and incomplete fusion cross sections in the sub-barrier energy region.

(2) At energies above the Coulomb barrier, the single channel calculated σ_J is larger than that obtained by the converged CDCC calculation in angular momentum region around J_c but it becomes smaller at relatively higher J . Finally, the single channel calculation and the converged CDCC calculation provide close values for the total fusion cross section, as shown in Fig. 16. It can be deduced that continuum coupling reduces and increases the probabilities of CF and ICF processes respectively in the above-barrier energy region.

As our present work overestimates the TF cross section at energies above the Coulomb barrier, we do not further investigate the continuum coupling effect on incomplete fusion in this paper. A comprehensive study of the continuum coupling effect on ${}^6\text{Li}$ fusion will be done in the future with a good description of CF, ICF and TF processes.

V. SUMMARY AND CONCLUSION

CDCC calculations have been presented for the fusion reactions of weakly bound projectile ${}^6\text{Li}$ with ${}^{28}\text{Si}$, ${}^{64}\text{Ni}$, ${}^{144}\text{Sm}$ and ${}^{209}\text{Bi}$ targets. The inclusion of continuum states up to 40 MeV was found necessary for the convergence of the total fusion cross sections, which means that the inclusion of closed channels in CDCC calculations is necessary for ${}^6\text{Li}$ fusion with light and medium mass targets, such as ${}^{28}\text{Si}$, ${}^{64}\text{Ni}$ and ${}^{144}\text{Sm}$, at incident energies around the Coulomb barriers. Reasonable agreement between the calculated TF cross section and experimental data is obtained.

At energies above the Coulomb barrier, it is found that the continuum coupling effects induced by low-energy ($0 \leq \varepsilon \leq 6.0$ MeV) and higher-energy ($6.0 \leq \varepsilon \leq 40.0$ MeV) continuum states are different for TF cross sections: the former reduces the TF cross sections by around 10-15%, but the latter increases the TF cross sections. Therefore the final converged results are nearly the same as the results of single channel calculations, in which no continuum coupling effects were taken into account.

In the sub-barrier region, the calculated TF cross section is further enhanced by including the higher-energy continuum states.

The Sum-rule model has been adopted to extract the complete fusion cross section as well as the critical angular momentum J_c . The coupling effect of continuum

states can not be ignored for the complete fusion process, especially at energies below the Coulomb barrier. In particular, the enhancement effect on the complete fusion cross section in the sub-barrier region is dominated by closed channels for the ${}^6\text{Li}+{}^{28}\text{Si}$, ${}^{64}\text{Ni}$ and ${}^{144}\text{Sm}$ systems. At energies above the Coulomb barrier, the CDCC calculated complete fusion cross section can be slightly enlarged by taking the higher-energy continuum states into account, while the converged result is still smaller than the single channel result. In general, the extracted suppression factors for complete fusion in the above-barrier region are consistent with previous studies for these reaction systems. It is found that the suppression mainly occurs in the angular momentum region $J_c - 2 \leq J \leq J_c$, which is independent of the fusion system. We believe that this independence calls for full-quantum investigations.

Finally, as the coupling effect of the higher-energy continuum states (including both open and closed channels) is remarkable for ${}^6\text{Li}$ induced fusion reactions, it is of interest to study their effect on the fusion reactions induced by other weakly bound nuclei, such as ${}^7\text{Li}$ and ${}^9\text{Be}$. Related research is in progress.

ACKNOWLEDGMENTS

This work was financially supported by the National Natural Science Foundation of China (Grant No. U2067205).

-
- [1] L. Canto, P. Gomes, R. Donangelo, and M. Hussein, Fusion and breakup of weakly bound nuclei, *Phys. Rep.* **424**, 1 (2006).
- [2] N. Keeley, N. Alamanos, K. Kemper, and K. Rusek, Elastic scattering and reactions of light exotic beams, *Prog. Part. Nucl. Phys.* **63**, 396 (2009).
- [3] K. Hagino and N. Takigawa, Subbarrier Fusion Reactions and Many-Particle Quantum Tunneling, *Phys. Rep.* **128**, 1061 (2012).
- [4] L. Canto, P. Gomes, R. Donangelo, J. Lubian, and M. Hussein, Recent developments in fusion and direct reactions with weakly bound nuclei, *Phys. Rep.* **596**, 1 (2015).
- [5] J. Lei and A. M. Moro, Puzzle of complete fusion suppression in weakly bound nuclei: A trojan horse effect?, *Phys. Rev. Lett.* **122**, 042503 (2019).
- [6] C. Beck, F. A. Souza, N. Rowley, S. J. Sanders, N. Aissaoui, E. E. Alonso, P. Bednarczyk, N. Carlin, S. Courtin, A. Diaz-Torres, A. Dummer, F. Haas, A. Hachem, K. Hagino, F. Hoellinger, R. V. F. Janssens, N. Kintz, R. Liguori Neto, E. Martin, M. M. Moura, M. G. Munhoz, P. Papka, M. Rousseau, A. Sánchez i Zafra, O. Stézowski, A. A. Suaide, E. M. Szanto, A. Szanto de Toledo, S. Szilner, and J. Takahashi, Near-barrier fusion of weakly bound ${}^6\text{Li}$ and ${}^7\text{Li}$ nuclei with ${}^{59}\text{Co}$, *Phys. Rev. C* **67**, 054602 (2003).
- [7] M. Dasgupta, P. R. S. Gomes, D. J. Hinde, S. B. Moraes, R. M. Anjos, A. C. Berriman, R. D. Butt, N. Carlin, J. Lubian, C. R. Morton, J. O. Newton, and A. Szanto de Toledo, Effect of breakup on the fusion of ${}^6\text{Li}$, ${}^7\text{Li}$, and ${}^9\text{Be}$ with heavy nuclei, *Phys. Rev. C* **70**, 024606 (2004).
- [8] P. K. Rath, S. Santra, N. L. Singh, R. Tripathi, V. V. Parkar, B. K. Nayak, K. Mahata, R. Palit, S. Kumar, S. Mukherjee, S. Appannababu, and R. K. Choudhury, Suppression of complete fusion in the ${}^6\text{Li}+{}^{144}\text{Sm}$ reaction, *Phys. Rev. C* **79**, 051601(R) (2009).
- [9] M. S. Gautam, K. Vinod, S. Duhan, R. P. Chahal, and H. Khatri, Investigation of contribution of complete and incomplete fusion in the total fusion process of ${}^6\text{Li}+{}^{90,96}\text{Zr}$ reactions in vicinity of the coulomb barrier, *Nucl. Phys. A* **998**, 121730 (2020).
- [10] Chetna, M. M. Shaikh, P. Singh, and R. Kharab, Exploring the effects of breakup couplings for weakly bound projectile ${}^9\text{Be}$ on various targets at around barrier energies, *Nucl. Phys. A* **1021**, 122418 (2022).
- [11] A. Diaz-Torres, I. J. Thompson, and C. Beck, How does breakup influence the total fusion of ${}^{6,7}\text{Li}$ at the coulomb barrier?, *Phys. Rev. C* **68**, 044607 (2003).
- [12] A. G. Camacho, A. Diaz-Torres, and H. Q. Zhang, Comparative study of the effect of resonances of the weakly bound nuclei ${}^{6,7}\text{Li}$ on total fusion with light to heavy mass targets, *Phys. Rev. C* **99**, 054615 (2019).
- [13] J. Lubian, J. L. Ferreira, J. Rangel, M. R. Cortes, and L. F. Canto, Fusion processes in collisions of ${}^6\text{Li}$ beams

- on heavy targets, *Phys. Rev. C* **105**, 054601 (2022).
- [14] E. de Barbará, G. V. Martí, A. Arazi, O. A. Capurro, J. O. Fernández Niello, J. M. Figueira, A. J. Pacheco, M. Ramírez, M. D. Rodríguez, J. E. Testoni, M. Verruno, I. Padrón, P. R. S. Gomes, and E. Crema, Fusion cross sections for the $6,7\text{Li}+27\text{Al}$, $9\text{Be}+27\text{Al}$ systems, *AIP Conference Proceedings* **884**, 189 (2007).
- [15] M. Sinha and J. Lubian, Small suppression of the complete fusion of ${}^6\text{Li} + {}^{28}\text{Si}$ reaction at near barrier energies, *Eur. Phys. J. A* **53**, 224 (2017).
- [16] C. S. Palshetkar, S. Thakur, V. Nanal, A. Shrivastava, N. Dokania, V. Singh, V. V. Parkar, P. C. Rout, R. Palit, R. G. Pillay, S. Bhattacharyya, A. Chatterjee, S. Santra, K. Ramachandran, and N. L. Singh, Fusion and quasi-elastic scattering in the ${}^{6,7}\text{Li}+{}^{197}\text{Au}$ systems, *Phys. Rev. C* **89**, 024607 (2014).
- [17] M. Dasgupta, D. J. Hinde, K. Hagino, S. B. Moraes, P. R. S. Gomes, R. M. Anjos, R. D. Butt, A. C. Berriman, N. Carlin, C. R. Morton, J. O. Newton, and A. Szanto de Toledo, Fusion and breakup in the reactions of ${}^6\text{Li}$ and ${}^7\text{Li}$ nuclei with ${}^{209}\text{Bi}$, *Phys. Rev. C* **66**, 041602(R) (2002).
- [18] K. Hagino, A. Vitturi, C. H. Dasso, and S. M. Lenzi, Role of breakup processes in fusion enhancement of drip-line nuclei at energies below the coulomb barrier, *Phys. Rev. C* **61**, 037602 (2000).
- [19] A. Diaz-Torres and I. J. Thompson, Effect of continuum couplings in fusion of halo ${}^{11}\text{Be}$ on ${}^{208}\text{Pb}$ around the coulomb barrier, *Phys. Rev. C* **65**, 024606 (2002).
- [20] S. Hashimoto, K. Ogata, S. Chiba, and M. Yahiro, New Approach for Evaluating Incomplete and Complete Fusion Cross Sections with Continuum-Discretized Coupled-Channels Method, *Prog. Theor. Phys.* **122**, 1291 (2009).
- [21] V. V. Parkar, V. Jha, and S. Kailas, Exploring contributions from incomplete fusion in ${}^{6,7}\text{Li}+{}^{209}\text{Bi}$ and ${}^{6,7}\text{Li}+{}^{198}\text{Pt}$ reactions, *Phys. Rev. C* **94**, 024609 (2016).
- [22] A. Gómez Camacho, B. Wang, and H. Q. Zhang, Systematic continuum-discretized coupled-channels calculations of total fusion for ${}^6\text{Li}$ with targets ${}^{28}\text{Si}$, ${}^{59}\text{Co}$, ${}^{96}\text{Zr}$, ${}^{198}\text{Pt}$, and ${}^{209}\text{Bi}$: Effect of resonance states, *Phys. Rev. C* **97**, 054610 (2018).
- [23] J. Rangel, M. Cortes, J. Lubian, and L. Canto, Theory of complete and incomplete fusion of weakly bound systems, *Physics Letters B* **803**, 135337 (2020).
- [24] M. R. Cortes, J. Rangel, J. L. Ferreira, J. Lubian, and L. F. Canto, Complete and incomplete fusion of ${}^7\text{Li}$ projectiles on heavy targets, *Phys. Rev. C* **102**, 064628 (2020).
- [25] M. Yahiro, Y. Iseri, H. Kameyama, M. Kamimura, and M. Kawai, Chapter III. Effects of Deuteron Virtual Breakup on Deuteron Elastic and Inelastic Scattering, *Prog. Theor. Phys. Suppl.* **89**, 32 (1986).
- [26] K. Ogata and K. Yoshida, Applicability of the continuum-discretized coupled-channels method to the deuteron breakup at low energies, *Phys. Rev. C* **94**, 051603(R) (2016).
- [27] W. Chen, H. Guo, T. Ye, Y. Ying, W. Sun, and Y. Han, Application of the lagrange-mesh method in continuum-discretized coupled-channel calculations, *J. Phys. G: Nucl. Part. Phys.* **49**, 075104 (2022).
- [28] J. Wilczyński, Calculations of the critical angular momentum in the entrance reaction channel, *Nucl. Phys. A* **216**, 386 (1973).
- [29] J. Wilczyński, K. Siwek-Wilczyńska, J. van Driel, S. Gonggrijp, D. C. J. M. Hageman, R. V. F. Janssens, J. Lukasiak, and R. H. Siemssen, Incomplete-fusion reactions in the ${}^{14}\text{N}+{}^{159}\text{Tb}$ system and a "sum-rule model" for fusion and incomplete-fusion reactions, *Phys. Rev. Lett.* **45**, 606 (1980).
- [30] J. Wilczynski, K. Siwek-Wilczynska, J. Van Driel, S. Gonggrijp, D. Hageman, R. Janssens, J. Lukasiak, R. Siemssen, and S. Van Der Werf, Binary l-matched reactions in ${}^{14}\text{N} + {}^{159}\text{Tb}$ collisions, *Nucl. Phys. A* **373**, 109 (1982).
- [31] B. Mukeru, M. Lekala, J. Lubian, and L. Tomio, Theoretical analysis of ${}^8\text{Li} + {}^{208}\text{Pb}$ reaction and the critical angular momentum for complete fusion, *Nucl. Phys. A* **996**, 121700 (2020).
- [32] B. Mukeru and L. Tomio, Analysis of fusion cross sections in the ${}^9\text{Be}$ projectile breakup on different target nuclei, *Braz J Phys* **51**, 157 (2021).
- [33] D. Tilley, C. Cheves, J. Godwin, G. Hale, H. Hofmann, J. Kelley, C. Sheu, and H. Weller, Energy levels of light nuclei $A=5, 6, 7$, *Nucl. Phys. A* **708**, 3 (2002).
- [34] P. Schmelzbach, W. Grüebler, V. König, and P. Marmier, Phase-shift analysis of d- α elastic scattering, *Nucl. Phys. A* **184**, 193 (1972).
- [35] W. Grüebler, P. Schmelzbach, V. König, R. Risler, and D. Boerma, Phase-shift analysis of d- α elastic scattering between 3 and 17 MeV, *Nucl. Phys. A* **242**, 265 (1975).
- [36] B. Jenny, W. Grüebler, V. König, P. Schmelzbach, and C. Schweizer, Phase-shift analysis of d- α elastic scattering between 3 and 43 MeV, *Nucl. Phys. A* **397**, 61 (1983).
- [37] S. Saito, Interaction between Clusters and Pauli Principle*, *Progress of Theoretical Physics* **41**, 705 (1969).
- [38] H. Horiuchi, Chapter III. Kernels of GCM, RGM and OCM and Their Calculation Methods, *Progress of Theoretical Physics Supplement* **62**, 90 (1977).
- [39] Y. Sakuragi, M. Yahiro, and M. Kamimura, Chapter VI. Microscopic Coupled-Channels Study of Scattering and Breakup of Light Heavy-Ions, *Prog. Theor. Phys. Suppl.* **89**, 136 (1986).
- [40] H. Guo, Y. Watanabe, T. Matsumoto, K. Ogata, and M. Yahiro, Systematic analysis of nucleon scattering from ${}^{6,7}\text{Li}$ with the continuum discretized coupled channels method, *Phys. Rev. C* **87**, 024610 (2013).
- [41] A. Koning and J. Delaroche, Local and global nucleon optical models from 1 KeV to 200 MeV, *Nucl. Phys. A* **713**, 231 (2003).
- [42] J. Bergstrom, 6li electromagnetic form factors and phenomenological cluster models, *Nuclear Physics A* **327**, 458 (1979).
- [43] I. Tanihata, H. Hamagaki, O. Hashimoto, Y. Shida, N. Yoshikawa, K. Sugimoto, O. Yamakawa, T. Kobayashi, and N. Takahashi, Measurements of interaction cross sections and nuclear radii in the light p -shell region, *Phys. Rev. Lett.* **55**, 2676 (1985).
- [44] N. Austern, Y. Iseri, M. Kamimura, M. Kawai, G. Rawitscher, and M. Yahiro, Continuum-discretized coupled-channels calculations for three-body models of deuteron-nucleus reactions, *Phys. Rep.* **154**, 125 (1987).
- [45] I. J. Thompson, Coupled reaction channels calculations in nuclear physics, *Comput. Phys. Rep.* **7**, 167 (1988).
- [46] M. Rhoades-Brown and P. Braun-Munzinger, Explanation of sub-barrier fusion enhancement in a coupled channels model, *Physics Letters B* **136**, 19 (1984).

- [47] L. Chamon, B. Carlson, and L. Gasques, São Paulo potential version 2 (SPP2) and Brazilian nuclear potential (BNP), *Computer Physics Communications* **267**, 108061 (2021).
- [48] B. V. Carlson and D. Hirata, Dirac-hartree-bogoliubov approximation for finite nuclei, *Phys. Rev. C* **62**, 054310 (2000).
- [49] T. Druet, D. Baye, P. Descouvemont, and J.-M. Sparenberg, CDCC calculations with the Lagrange-mesh technique, *Nuclear Physics A* **845**, 88 (2010).
- [50] T. Druet and P. Descouvemont, Continuum Effects in the Scattering of Exotic Nuclei, *Eur. Phys. J. A* **48**, 147 (2012).
- [51] D. Baye, The lagrange-mesh method, *Phys. Rep.* **565**, 1 (2015), the Lagrange-mesh method.
- [52] M. M. Shaikh, S. Roy, S. Rajbanshi, M. K. Pradhan, A. Mukherjee, P. Basu, S. Pal, V. Nanal, R. G. Pillay, and A. Shrivastava, Investigation of ${}^6\text{Li} + {}^{64}\text{Ni}$ fusion at near-barrier energies, *Phys. Rev. C* **90**, 024615 (2014).
- [53] A. Pakou, K. Rusek, N. Alamanos, X. Aslanoglou, M. Kokkoris, A. Lagoyannis, T. J. Mertzimekis, A. Musumarra, N. G. Nicolis, D. Pierroutsakou, and D. Roubos, Total reaction and fusion cross sections at sub- and near-barrier energies for the system ${}^7\text{Li} + {}^{28}\text{Si}$, *Eur. Phys. J. A* **39**, 187 (2009).
- [54] M. Sinha, H. Majumdar, P. Basu, S. Roy, R. Bhattacharya, M. Biswas, M. K. Pradhan, R. Palit, I. Mazumdar, and S. Kailas, Sub- and above-barrier fusion of loosely bound ${}^6\text{Li}$ with ${}^{28}\text{Si}$, *Eur. Phys. J. A* **44**, 403 (2010).
- [55] M. Hugi, J. Lang, R. Müller, E. Ungricht, K. Bodek, L. Jarczyk, B. Kamys, A. Magiera, A. Strzałkowski, and G. Willim, Fusion and direct reactions for strongly and weakly bound projectiles, *Nuclear Physics A* **368**, 173 (1981).
- [56] P. K. Rath, S. Santra, K. Mahata, R. Tripathi, V. V. Parkar, R. Palit, and N. L. Singh, Complete versus incomplete fusion in ${}^6\text{Li} + {}^{144}\text{Sm}$ reaction, *Proceedings of the International Symposium on Nuclear Physics*, 310 (2009).